PGM-free $CuO/LaCoO_3$ nanocomposites: new opportunities for TWC application

M. Pacella[a], A. Garbujo[a], J. Fabro[b], M. Guiotto[b], Q. Xin[c], M.M. Natile[d], P. Canu[b], P. Cool[c], A. Glisenti[a,d]*

[a] Department of Chemical Sciences, University of Padova, - Via F. Marzolo, 1, 35131, Padova, Italy.

[b] Department of Industrial Engineering, University of Padova - Via F. Marzolo, 9, 35131, Padova, Italy.

[c] Laboratory of Adsorption and Catalysis - Department of Chemistry - University of Antwerp, Universiteitsplein 1 – 2610 Wilrijk, Belgium

[d] Institute of Condensed Matter Chemistry and Technologies for Energy (ICMATE), National Research Council (CNR) c/o Department of Chemical Sciences, University of Padova - Via F. Marzolo 1, 35131, Padova, Italy.

Keywords: TWC, PGM-free catalysts, CO assisted NO reduction, $LaCoO_3$-based nanocomposites, Ammonia-Driving Deposition Precipitation (ADP).

* Corresponding author: Dr. Marta Maria Natile, PhD

Institute of Condensed Matter Chemistry and Technologies for Energy (ICMATE), National Research Council (CNR) c/o Department of Chemical Sciences, University of Padova - Via F. Marzolo, 1, 35131, Padova, Italy. Phone n. +39 049 8275196 – Fax +39 049 8275829 – E-mail: martamaria.natile@unipd.it.

Abstract

In this contribution several $LaCoO_3$ based nanocomposites have been prepared and tested for application as Three-Way Catalytic Converters (TWC): the aim is in developing Platinum Group Metal (PGM)-free catalysts. To reach this objective we designed and realized nanocomposites in which active CuO nanoparticles are deposited on active $LaCoO_3$. This perovskite is active in oxidation while copper is active in reduction: catalytic bifunctionality is thus built-in via a tailor-made and controlled nanocomposition. The deposition was carried out by means of an innovative Ammonium-Driving-Deposition precipitation (ADP) procedure allowing to obtain nanocomposites in which CuO is highly dispersed on $LaCoO_3$. This increases the reducibility of the nanocomposites, as revealed by the TPR measurements. The deposition of copper does not alter significantly the surface composition which remains rich in lanthanum oxide/hydroxide, the main effect consisting in a slight increment of surface hydroxylation. Moreover, the copper amount on the $LaCoO_3$ surface does not increase linearly with the nominal composition but reaches a plateau.

Both model reactions (CO oxidation and CO assisted NO reduction) and tests with a synthetic automotive exhaust mixture, including 10% steam, were carried out. Activity before and after high-temperature aging in steam was also evaluated. We compared the obtained results with the ones of CuO/nickelates of a previous work, to highlight the functionalities gained.

In simple CO+NO and CO+O_2 mixtures, the deposition of copper oxide on $LaCoO_3$ greatly increases the activity of the nanocomposites in NO reduction (100% conversion at 350°C) without significantly affecting the reactivity in CO oxidation. Results with the synthetic automotive exhaust mixture show that Cu loading on ADP-prepared catalysts can significantly improve the NO reduction activity of $LaCoO_3$. Still, NO reduction remains more relevant in O_2-poor mixtures (about 100% conversion around 400°C in the 10% Cu loaded), even slightly below the stoichiometric. Some deactivation on hydrocarbon oxidations occurs at low temperatures due to thermal aging, apparently due to coking and surface Cu depletion. Compared to CuO deposited by ADP on $LaNiO_3$ of our earlier studies, cobaltites gain in oxidation activity, but NO reduction remains easier on nickelates. However, the promising performance and the absence of noble critical metals are promising features to develop PGM-free catalysts for the automotive industry.

1. Introduction

Among perovskites, lanthanum cobaltite has been observed to be active in oxidation [1]. Although Libby suggested in 1971 the possible use of $LaCoO_3$ as a catalyst in Three Way Catalysts (TWC), [2] the materials for automotive are still based on noble metals (Platinum Metal Group – PGM). Nowadays, the development of innovative catalysts in which the use of PGMs is reduced or avoided is fundamental considering the cost and the problems related to the limited supply. Several researchers focused on perovskite-based catalysts for exhaust control trying to enhance catalytic activity by means of doping [3-9]. For this purpose it has to be considered that NO reduction is still the most difficult outcome to be achieved (even more considering the need to decrease or avoid the use of noble metals). In our previous study, we discovered an enhanced NO reduction activity by doping $LaCoO_3$ with copper [10]. In the

$LaCo_{1-x}Cu_xO_3$ catalysts the presence of copper inside the perovskitic lattice increases the oxygen vacancies and mobility [10-11] that are considered to play a significant role in the NO reduction. A crucial step in NO reduction on perovskites, in fact, is NO dissociative adsorption, which is particularly difficult at low temperature [12]; considering that NO interacts dissociatively with oxygen vacancies, doping with copper, should favor the formation of vacancies [13] and increases the reactivity of perovskites with respect to NO reduction [10]. Oxygen mobility is important because it can also favor the conversion of CO into CO_2, whereas cations reducibility can facilitate the CO_2 desorption, preventing the catalyst deactivation. Oxygen vacancies and mobility are a consequence of the insertion of copper inside the perovskitic cell but also the effect of the presence of copper species surface segregated on perovskite reducibility should be considered. Tien-Thao et al. [11,14], in fact, hypothesized that under reducing conditions copper diffuses towards the surface acting as a catalyst for hydrogen dissociation and enhancing reducibility, particularly for grain boundaries species. The surface segregation of copper on the perovskite surface was frequently observed under reaction conditions; moreover, traces of highly dispersed copper oxide have been revealed on the surface of largely Cu-doped $LaCo_{1-x}Cu_xO_3$ perovskites. These observations suggest that surface dispersed copper oxide could play a role in reactivity.

Many composite catalysts with copper oxide supported on other metal oxides are used in different reactions, including steam reforming and oxidative steam reforming of alcohols [15], preferential CO oxidation [16-18], methanol synthesis [19, 20]. In these reactions, the best performances are obtained when copper is highly dispersed [15]. Inspired by those evidences, we investigated $CuO/LaCoO_3$ nanocomposite materials in which copper oxide is highly dispersed on the surface of $LaCoO_3$. Several nanocomposites were synthesized, by depositing different

amount of copper oxide on $LaCoO_3$ and carefully characterized by means of X-Ray Photoelectron Spectroscopy (XPS), X-Ray Diffraction (XRD), BET, Temperature Programmed Reduction (TPR), Scanning Electron Microscopy (SEM), and Energy Dispersive X-Ray (EDX) analysis, Inductive Coupled Plasma Optical Emission Spectrometry (ICP-OES), and Transmission Electron Microscopy (TEM).

For the copper deposition onto the perovskite, we applied an innovative ammonia based impregnation method. The so-called ammonia driven deposition precipitation method was first reported by Guo *et. al*. as a simple and efficient preparation approach for silica supported copper catalysts [21]. The formation of copper tetra-ammonia complex $[Cu(NH_3)_4(H_2O)_2]^{2+}$ provides an excellent steric hindrance between the individual Cu ions. The overall result after the calcination is a well dispersed CuO phase on to the surface of supporting material. In the current paper, we optimize and adapt the existing method in order to enhance the dispersion degree on perovskite surfaces. For comparison, a Cu loaded $LaCoO_3$ catalyst was also prepared by using the conventional wet impregnation method.

The effect of copper oxide deposition on the reactivity of $LaCoO_3$ was investigated in CO oxidation and in CO assisted NO reduction. Beside this, the TWC activity with complex mixtures simulating an automotive exhaust was also tested, in order to evaluate the effective applicability of such catalytic materials. The mixtures include steam, CO_2 and hydrocarbons: exhaust composition and temperature can severely differ with respect to common laboratory conditions (eg. large NO and CO concentrations, lack of O_2) being extremely challenging to prove the effective activity of the nanocomposites. Sulphur effects have not been addressed at this stage of investigation. Although ultra-low (10-15 ppm) [22] and sulphur-free [23] fuels are spreading, and technologies to remove sulphur oxides upstream of the catalyst converter are in

use [24], resistance of novel catalytic materials to sulphur poisoning remains an issue. It will be investigated on catalysts where HC and oxidation, and NO reduction activity proved competitive with current TWC catalysts. Thermal deactivation is also a challenge for industrial scaling [25, 26], possibly causing sintering of the catalytic particles, decrease of catalytic surface area, coking. In this work the resistance to thermal degradation was investigated by a protocol that cycles the catalyst temperature from RT up to 800°C, for several hours.

We already studied the performances of several nanocomposites obtained depositing via ADP different amounts of CuO on $LaNiO_3$ [27], to match the reduction capability of copper with the activity in oxidation of perovskite. In the present work, the catalytic activity of Cu-doped cobaltites vs nickelates is also discussed.

2. Experimental

2.1 Synthesis

2.1.1 Synthesis of $LaCoO_3$ support

The perovskite support was synthesized with the conventional citrate route [10]. Briefly, citric acid monohydrate (Sigma-Aldrich ≥ 99.0%) was added to the aqueous solution of the cations precursors (obtained by mineralization with nitric acid (Sigma-Aldrich 65.0 %) the stoichiometric amounts of the corresponding oxides, La_2O_3 (Sigma-Aldrich 99.9%) and CoO (Acros 99%), respectively) under vigorous stirring. The total number of moles of cations to that of citric acid was 1:1.9. The solution was heated at 80°C in a water bath to promote solvent evaporation and obtain a wet-gel, which was then treated at 400°C for 2 hours in air to

decompose the organic framework. The ash-like material was finally grinded and calcined in air at 650°C with 6°C/min of heating rate for 6 hours to obtain the desired perovskite phase.

2.1.2 Synthesis of the CuO/$LaCoO_3$ nanocomposites by ADP and by WI

CuO-loaded $LaCoO_3$ materials with increasing amount of copper were prepared by the Ammonium-Driving Deposition precipitation (ADP). Typically, 500 mg $LaCoO_3$ perovskite was suspended in 25 mL of de-ionized water containing the appropriate amounts of copper ($Cu(NO_3)_2 \bullet 3H_2O$, >99%, Merck) and ammonia (NH_4OH, 28-30 %, Sigma Aldrich) with a molar Cu/NH_3 ratio of 1/6. The whole suspension was then stirred for 48 h at room temperature, followed by a drying step at 60°C overnight. After cooling, the dried samples were calcined at 550°C for 8 h with a heating rate of 1°C/min. The samples were denoted as CuX, where the X represents the amount copper in weight % (Table 1).

As reference, a CuO/$LaCoO_3$ sample containing 15 wt.% of Cu was also prepared by the conventional wet impregnation (WI) method. In this method $LaCoO_3$ was added into a 25 mL solution containing a required amount of $Cu(NO_3)_2 \bullet 3H_2O$ (> 99%, Merck) so that the metal loading reached 15 wt.% in the final catalyst. The mixture was stirred at room temperature for 48 h and dried at 60°C overnight. Finally, the solid was calcined at 550 °C with a heating rate of 1°C/min for 6 h. The synthesized samples are summarized in Table 1.

Table1: BET Specific Surface Area, Cu/Co ICP atomic ratios, as a function of the nominal composition for the $CuO/LaCoO_3$ nanocomposites.

Sample	Deposition method[a]	Sample name[b]	Cu/Co[c]	Cu/Co[d] (ICP)	S_{BET} (m^2/g)
$LaCoO_3$	-	$LaCoO_3$			17.9
10% wt. Cu on $LaCoO_3$	ADP	Cu10	0.4	0.4	11.6
15% wt. Cu on $LaCoO_3$	ADP	Cu15	0.6	0.5	9.1
20% wt. Cu on $LaCoO_3$	ADP	Cu20	0.8	0.8	9.8
30% wt. Cu on $LaCoO_3$	ADP	Cu30	1.1	1.0	8.9
15% wt. Cu on $LaCoO_3$	WI	Cu15 WI	0.6	0.4	6.4

[a] = Ammonium-Driving Deposition Precipitation (ADP) and Wet Impregnation (WI) procedures
[b] = short name used in this article
[c] = nominal, from precursors' weighted amounts.
[d] = from inductively coupled plasma optical emission spectrometry (ICP-OES).

2.2 Characterization

The XPS measurements were carried out with a Perkin Elmer Φ 5600ci Multi Technique System. The spectrometer was calibrated by assuming the binding energy (BE) of the Au $4f_{7/2}$ line to be 84.0 eV with respect to the Fermi level. Both extended spectra (survey - 187.85 eV pass energy, 0.5 $eV \cdot step^{-1}$, 0.05 $s \cdot step^{-1}$) and detailed spectra (for La 3d, Co 2p, Cu 2p, O 1s and C 1s – 23.50 eV pass energy, 0.1 $eV \cdot step^{-1}$, 0.1 $s \cdot step^{-1}$) were collected with a standard Al Kα source working at 250 W. The standard deviation in the BE values of the XPS line is 0.10 eV. The atomic percentage, after a Shirley-type background subtraction [28], was evaluated by using the PHI sensitivity factors [29]. The peak positions were corrected for the charging effects by considering the C 1s peak at 285.0 eV and evaluating the BE differences [30].

The XRD analyses were performed with a Bruker D8 Advance diffractometer with Bragg-Brentano geometry using a Cu Kα radiation (40 kV, 40 mA, λ = 0.154 nm). The data were collected each 0.03° at a counting time of 10 s/step in the (2θ) range from 10° to 90°. The crystalline phases were identified by the search-match method using the JCPDS database.

The TPR measurements were carried out with an Autochem II 2920 Micromeritics, equipped with a TCD detector, by using 50 mg of sample in a quartz reactor and heating from RT to 900°C at 10°C min^{-1} under a constant flow of H_2 at 5% in Ar (50 mL·min^{-1}). TPR samples were previously outgassed with He (50 mL·min^{-1}) at RT.

N_2 adsorption and BET specific surface area measurements were determined by Quantachrome Quadrasorb SI automated gas adsorption system. The measurements were carried out at liquid nitrogen temperature. The specific surface area was calculated using the Brunauer-Emmet-Teller (BET) equation. Prior to N_2-sorption, all samples were degassed at 200°C for 16 h. Field emission-scanning electron microscopy and EDX measures were carried on a Zeiss SUPRA 40VP. Morphological analysis was carried out setting the acceleration voltages between 17 and 18 kV, 20 kV have been used for EDX analysis.

Inductively coupled plasma optical emission spectrometry was performed with an ICP-OES Perkin Elmer Optima 4200 Dual View. The samples for ICP analysis were prepared by dissolving the powder (about 20 mg exactly weighted) in a solution of 10 mL of HCl (Sigma-Aldrich, ≥ 37%) and 10 mL HNO_3 (Sigma Aldrich, ≥ 65 %) under stirring at about 80°C for 2h.

TEM analysis was performed with Tecnai G2 (FEI) transmission electron microscope operating at 100 kV. Images were captured with a Veleta (Olympus Soft Imaging System) digital camera. Samples dispersed in ethanol were drop cast on carbon-coated grids (400 mesh Cu).

2.3 Catalytic tests

Two series of activity tests were carried out. The first set of measurements used simplified mixtures to understand the basic reaction mechanism. 40 mg of sample was loaded in a quartz

reactor of 6 mm internal diameter; the temperature was monitored by a thermocouple inserted right upstream of the bed. In this configuration we studied two model reactions: CO assisted NO reduction and CO oxidation. As reported in Table 2 both reactions, NO + CO and CO + O_2, were studied using a stoichiometric mixture of reactants and a total flow rate of 100 ml/min at atmospheric pressure. The inert carrier was always Ar. The flows were controlled by thermal mass flowmeters (Vögtlin Instruments). The temperature of the bed was varied between RT and 400°C with a stepped temperature program. The reaction products were monitored with an Agilent 7890A gas chromatograph, equipped with a TCD detector. The columns are a molecular sieve 13X (60/80 mesh, 1.8 m) and a Porapak Q (1.8 m). The calibration was done using standard gases containing known concentrations of the components.

The second set of activity measurements aimed at approaching actual conditions of an automotive exhaust, exploring the interferences of higher hydrocarbons, H_2, and large amount of steam and CO_2. The experimental set-up has been already presented [10]. The operating conditions were modified as described below and summarized in Table 2. We used a quartz flow reactor, 8 mm ID. The gas mixtures were measured by GC (Agilent 7820) with Porapak Q and MS5A packed columns in series; both TCD and FID detectors were used. The GC is online with the gas outlet and programmed to continuously sample the mixture, so that measurements can be collected at approx. each 10 min. A direct-access, 0-200 amu mass spectrometer (Hiden QID-20) was also used, to measure NO. The analysis with the MS is almost continuous (each less than 1 min). The feed mixture detailed in Table 2 is quite complex, trying to approximate a real automotive exhaust. The flow rates were controlled by a set of 6 thermal mass flow meters (Brooks Instruments and Bronkhorst High-Tech); H_2O was fed via an isothermal bubbler. Note that stoichiometry of O_2 is based on all the fuels plus the amount expected from NO conversion

to N_2 and O_2.

Table 2: Feed compositions used for the catalytic measurements.

Inert	CO_2	H_2O	O_2	CO	NO	H_2	CH_4	C_3H_6	C_3H_8	Λ^a		m_{cat}	Flow	GHSV[b]
(balance)	%[c]	%[c]	%[c]	%[c]	%[c]	%[c]	ppm	ppm	ppm			mg	SmL/min	1/h
Ar	-	-	-	4	4	-	-	-	-	-		40	100	150000
Ar	-	-	2	4	-	-	-	-	-	1.0	Stoich	40	100	150000
He	15	10	0.777	0.7	0.1	0.233	230	450	230	1.0	Stoich	200	200	60000
He	15	10	0.609	0.9	0.1	0.300	300	600	300	0.6	Rich	200	200	60000

[a] **Λ** = O_2 fed/O_2 stoichiometric = $[O_2]/(0.5\,[CO] + 0.5\,[H_2] + 2\,[CH_4] + 4.5\,[C_3H_6] + 5\,[C_3H_8] - 0.5\,[NO])$
[b] For GHSV we used a bulk density of 1 g/mL for all the powders.
[c] vol%

Note that 10 vol % of steam was always fed, reflecting actual conditions, quite challenging for the catalysts. The standard testing sequence in the second set of measurements proceeds through the steps: 1) heating the catalyst at 10°C/min up to 600°C, under flow of air, 2) 2h of pre-conditioning at 600°C in flowing air, 3) 1 h of conditioning at 600°C with reacting mixture without NO to identify on the MS the m/e=30 baseline (zero) partial pressure value, 4) 2 h of conditioning at 600°C with the complete reacting mixture, 5) slow temperature decrease (-2°C/min) to measure the catalyst activity at different temperatures. It has been verified that the selected cooling rate of -2°/min is sufficiently low to achieve steady-state operation of the catalyst, at each temperature scanned. The reaction temperature was monitored by a K-type thermocouple, 5 mm downstream of the catalytic bed.

Finally, catalyst thermal stability has been investigated. The aging protocol followed different steps, alternating low and high temperatures, up to 800°C. The stoichiometric mixture simulating the actual exhaust, including 10% of steam, was continuously fed during the whole sequence. The first step is the standard testing procedure used and described for ordinary activity test. A

second thermal cycle follows, in which the catalyst is rapidly brought up to 700°C, at 15°C/min and kept for 3 hours. After decreasing the temperature to 600°C, step 5) of the standard testing sequence is performed. Then, the catalyst is rapidly reheated to 800°C at 15°C/min and maintained at such temperature for 3 hours; finally step 5) follows. The catalyst activity was continuously monitored, including the high temperature steps. Total aging treatment took approx. 35 hours. The catalytic activity has been evaluated on the fresh sample and after each high-temperature treatment.

3. Results and discussion

3.1 Chemical, structural, and morphological characterization

Two phases can be identified in the diffraction patterns of the nanocomposite systems (Figure 1): the rhombohedral $LaCoO_3$ of the perovskite support and the monoclinic CuO (35.61° and 38.85°). The contributions of CuO become more evident as copper content increases (from 10 to 15%). In the Cu10 sample CuO peaks are not well defined, suggesting that copper is highly dispersed on the support. It is noteworthy that there is no shift of the patterns toward lower angle values with respect to the $LaCoO_3$, indicating that Cu did not enter in the unit cell of the perovskite (see insert in Figure 1).

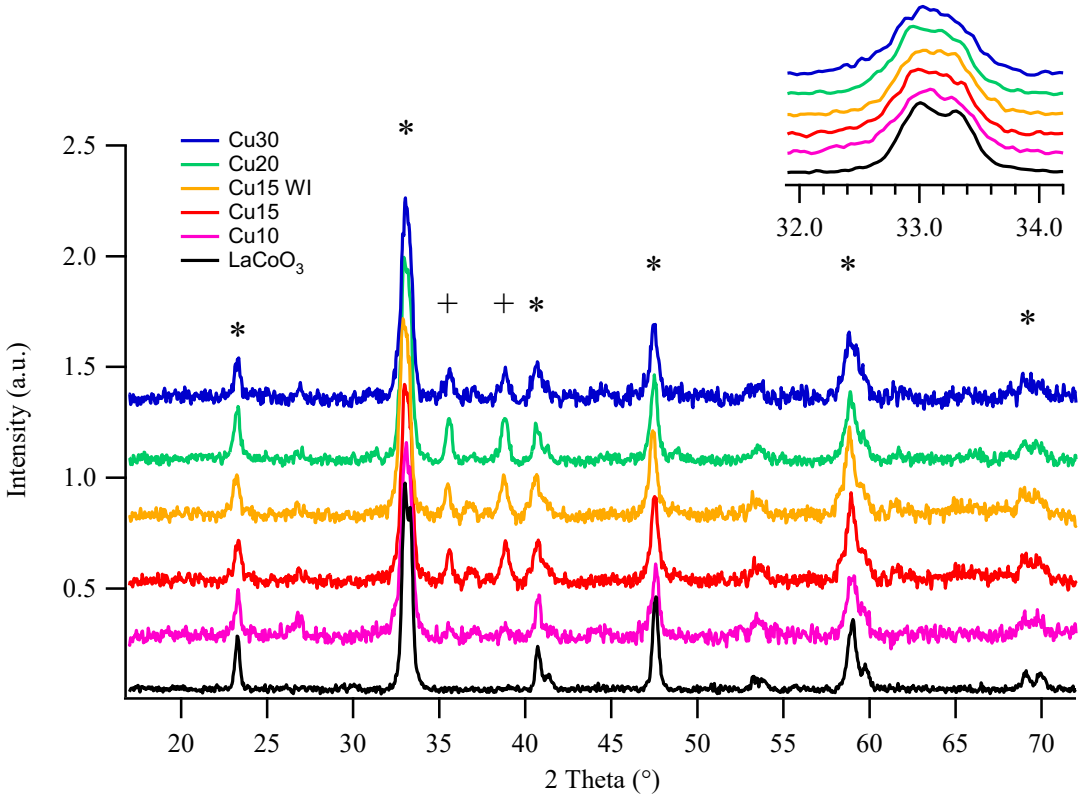

Figure 1: XRD patterns of the CuO/$LaCoO_3$ nanocomposites and of the $LaCoO_3$ support; in the insert a detail of the more intense signal of the perovskite.(+ = CuO; ∗= $LaCoO_3$).

The deposition of CuO on the $LaCoO_3$ is confirmed by the TEM images (Figure 2) reported for Cu10 and Cu30 in order to underline the increment in the number of particles observed with increasing the deposited amount of copper. In Cu10 the deposited CuO particles are visible on the surface of the perovskitic grains; their dimension ranges around 10-12 nm. In the Cu30 sample the CuO particle are more difficult to distinguish being increased greatly in number; however, their dimension is similar to the Cu10 ones.

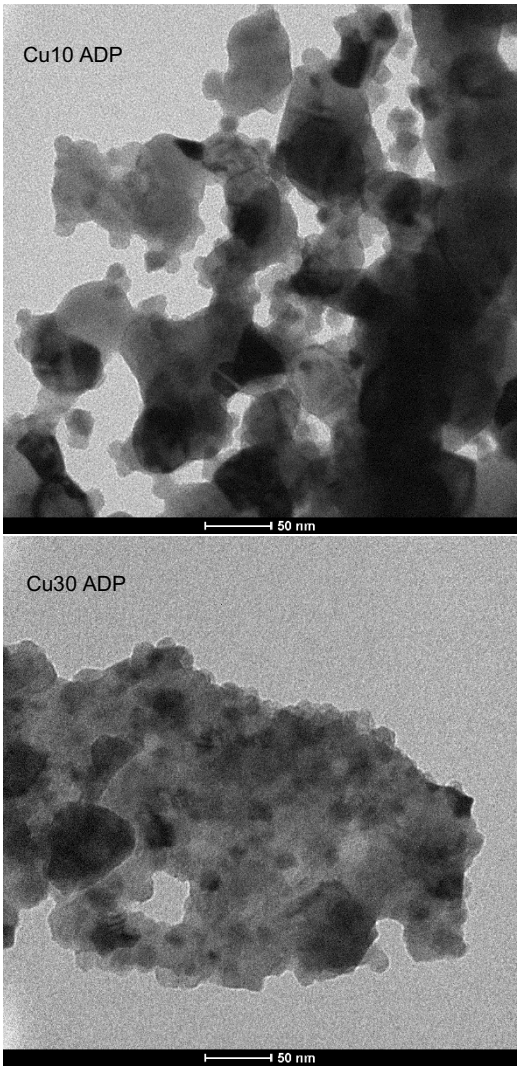

Figure 2: TEM images of the Cu10 and Cu30 prepared by ADP.

XPS spectra are reported in the Supporting Material (Figure S1). La 3d peaks shape (shake-up structures at about 838 and 855 eV [31-33]) and position suggest the presence of La(III). A careful analysis of La $3d_{5/2}$ reveals two components at 833.4-833.6 and 834.6-834.9 eV. The comparison with literature suggests their attribution to the perovskite (833.2 eV) [34-35] and to hydroxide/oxide species such as $La(OH)_3$ (835.0 eV) and LaOOH (834.8 eV) [31-33, 36-38]. In the Co 2p spectra both the peak positions (779.8-780.6 and 795.2-795.5 eV) and shape (absence of the shake-up contribution at about 786-788 eV) are consistent with the presence of Co(III) [30,32-34].

La 3d and Co 2p XPS regions are not significantly affected by the deposition of Cu: no relevant differences can be revealed between the bare support and the nanocomposites. Only in the higher Cu containing composite (Cu30) a broadening toward higher BE values of the La $3d_{5/2}$ and Co $2p_{3/2}$ peaks can be observed, indicating some hydroxylation of the surface (lanthanum and cobalt hydroxylation) and a different chemical surrounding. The Cu 2p peaks shape and position are consistent with the presence of Cu(II), as confirmed by the shake-up contributions at 942-943 eV and 962-963 eV. The position of the Cu $2p_{3/2}$ signal (933.2-934.2 eV) is in accordance with the standard binding energy of Cu(II) in CuO [29]. Only in the Cu10 the lower intensity of the shake-up contribution suggests also the presence of Cu(I) [29]. Consistently, the position of the Cu $2p_{3/2}$ peak shifted toward slightly lower BE (933.2 instead of 934.1 eV). Two main signals compose the O 1s spectra: the peak at 528.9-529.6 eV is characteristic of the lattice oxygen in metal oxides whereas the one at 531.3-531.8 eV can be attributed to oxygen in hydroxides and carbonates [30-33]. In general this latter contribution becomes more evident with increasing the amount of copper, suggesting a higher hydroxylation of the surface, as confirmed also by the higher amount of oxygen present in the Cu30 sample (Table 3). The main difference observed in

the sample prepared by Wet Impregnation is the more evident presence of lanthanum oxide/hydroxide species (contribution around 835 eV) and of the O 1s contribution due to hydroxide/carbonate species. The XPS quantitative analysis (Table 3) reveals, as expected, that Lanthanum is surface segregated in the supporting $LaCoO_3$ (La/Co atomic ratio = 1.7). This is strictly a surface phenomenon as confirmed by the EDX composition which is near the nominal one (EDX La/Co atomic ratio = 1.1). The deposition of copper does not change this behavior and lanthanum results surface segregated in all the nanocomposites (La/Co atomic ratio around 1.5-1.6). Concerning the nanocomposite prepared by ADP, the Cu amount on the surface, determined by means of XPS, increases with Cu loading but not as expected. The Cu/La atomic ratios, in fact, are always lower than the nominal ones. This trend suggests a slight diffusion of the copper in the subsurface layers. This hypothesis was confirmed by EDX. EDX sampling depth, in fact, is higher than XPS one (around 1 μm vs 50−100 Å for XPS) and reveals that the Cu/Co and Cu/La atomic ratios values are in good agreement with nominal ones (within the experimental error). The EDX values are also in agreement with ICP data (see Table 1). The limited diffusion of the copper, confirms that there is no shift of perovskite diffraction patterns. If we compare the XPS quantitative data of the Cu15 ADP with the analogous Cu15 WI it is evident that ADP allows to deposit a higher amount of copper on the perovskite surface.

Table 3: XPS and EDX atomic compositions obtained for $LaCoO_3$ and $CuO/LaCoO_3$ nanocomposites; inside brackets the atomic composition determined considering only the cations are reported. The nominal compositions (from the weighted amounts) are reported for comparison.

Samples		La	Co	Cu	O	La/Co	Cu/Co	Cu/La
$LaCoO_3$	XPS	17 (62)	10 (38)	-	73	1.7	-	-
	EDX	23.0 (52)	22 (48)	-	55	1.1	-	-
	Nominal	20 (50)	20 (50)	-	60	1.0	-	-
Cu10	XPS	17 (55)	11 (35)	3 (10)	69	1.5	0.3	0.2
	EDX	17 (40)	18 (43)	7 (17)	58	0.9	0.4	0.4
	Nominal	17 (42)	17 (42)	7 (16)	59	1.0	0.4	0.4
Cu15	XPS	20 (51)	12 (31)	7 (18)	61	1.6	0.6	0.4
	EDX	18 (38)	19 (40)	11 (23)	52.0	0.9	0.6	0.6
	Nominal	16 (38)	16 (38)	10 (24)	58	1.0	0.6	0.6
CU15 WI	XPS	15 (52)	10 (34)	4 (14)	71	1.5	0.4	0.3
	EDX	13 (31)	17 (40)	12 (29)	58	0.8	0.7	0.9
	Nominal	16 (38)	16 (38)	10 (24)	58	1.0	0.6	0.6
Cu20	XPS	16 (49)	9 (27)	8 (24)	67	1.8	0.9	0.5
	EDX	15 (33)	17 (37)	14 (30)	54	0.9	0.8	0.9
	Nominal	15 (36)	15 (36)	12 (28)	58	1.0	0.8	0.8
Cu30	XPS	12 (44)	8 (30)	7 (26)	73	1.5	0.9	0.6
	EDX	14 (29)	16 (33)	18 (38)	52	0.9	1.1	1.3
	Nominal	14 (32)	14 (32)	16 (36)	56	1.0	1.1	1.1

3.2 N_2 Sorption

The adsorption-desorption isotherms of the samples (Supporting Material - Figure S2) reveal, according to the IUPAC classification, that all of the samples exhibit type V isotherms accompanied by a type H3 hysteresis loop. Typically for the perovskite materials, the samples contain only non-rigid aggregates of sheet-like particles which give rise to slit-shaped pores.

This aggregated morphology is confirmed by the SEM image of the $LaCoO_3$ (Supporting Material – Figure S3). It is interesting to notice a drop of the BET specific surface area (Table 1) with increasing of copper content deposited onto the perovskite. This drop is caused by the CuO particles which cover the support's surface entering into the slit-shaped pores. This behavior is in line with the XPS, EDX and ICP compositions and is consistent with the morphology changes observed in SEM images.

On the other hands, catalyst prepared by the conventional WI method seemed to have a poor dispersion of the metal oxide particles and, in spite of the lower copper content, the morphology is not deeply different with respect to Cu30 prepared by ADP. Moreover, the surface area of the sample obtained by WI has a strong decrease of 64 % while it is only 50 % for ADP sample. This significant difference indicates that ADP is a superior impregnation method compared to WI for guaranteeing a good dispersion state of the metal oxide on the surface. Evidently, it is also expected that the ADP sample will have a better catalytic activity.

3.3 Temperature Programmed Reduction

The redox behavior of the $CuO/LaCoO_3$ materials is determined by H_2-TPR measurement (Table 4 and Supporting Material – Figure S4).

For the pure $LaCoO_3$ support, mainly two reduction signals can be observed. The broad band centered at around 440°C is attributed to the reduction of Co(III) to Co(II), while the second reduction peak centered at 600 °C with a tail at a higher temperature can be ascribed to the further reduction of Co(II) to Co(0). These results agree with literature: Co(III) is reduced to Co(II) at about 400-440°C, the complete reduction of Co(II) to Co(0) takes place at higher temperatures (620-670°C) [4, 39-44].

Focusing on the nanocomposites, it is clear that the deposition of copper oxide alters the redox properties of the catalysts. First, an additional reduction signal around 300-320°C can be observed, which is a good evidence of the presence of CuO on the surface and, consistently with the XRD results, it suggests that copper is not inside the perovskitic structure. Bulk CuO has, generally, been reported to reduce around 300°C [45]; in the present case, the reduction temperature observed for a reference commercial CuO sample was 316°C.

Beside the appearance of this signal, another difference concerns a shift of the peaks attributed to cobalt reduction which are observed to move from 440 to 400-420°C and from 600 to 560-580°C (Table 4, Peaks 2 and 3, respectively). The decrease of the cobalt reduction temperature in presence of copper was already observed in literature. Tien-Thao et al. [11,14] studying copper doped $LaCoO_3$ perovskites hypothesized that under reducing conditions copper exits from the perovskite cell and move toward the surface creating clusters that act as a catalysts for hydrogen dissociation. This causes the decrease of the Co(III) reduction temperature particularly for the

grain boundaries cobalt species. We observed the same behavior in $LaCo_{1-x}Cu_xO_3$ [10, 15, 46] in which the reduction temperatures shift at lower values with increasing copper content.

In this contribution, in contrast, copper oxide is deposited on the perovskite surface and a different behavior is expected. The deposition of copper oxide, even in lower amounts, facilitates the reduction of cobalt to Co(0). This phenomenon was also observed for the $LaCo_{1-x}Cu_xO_3$ perovskites, but in this case the effect was more significant on Co(III) and Co(II) reduction temperature (the temperature shift being around 140°C instead of 50°C). When copper is deposited on the perovskite surface instead of being inside the unit cell the temperature shift is less evident, but a relevant part of cobalt is reduced at oxidation states lower than Co(II) at around 420-440°C.

The H_2 consumption values determined for $LaCoO_3$ and for the $CuO/LaCoO_3$, catalysts are compared in Table 4. The values obtained for the total consumption are very similar to the ones calculated considering the presence of Cu(II) and Co(III). The deposition of copper, beside decreasing the reduction temperature, promotes cobalt reduction to oxidation states lower than Co(II) at 420-440°C, as revealed by the low relative intensity of the signal at higher temperature (named Peak 3); this behavior is much more evident than in $LaCo_{1-x}Cu_xO_3$ underlining the effect of the presence of surface dispersed copper on the reduction behavior of catalysts. The high intensity of the signal at 410-440°C with respect to the total amount of cobalt suggests that also copper reduction, to Cu(I) or Cu(0), contributes to this signal.

Table 4: TPR H_2 consumption data determined on $LaCoO_3$ and on the nanocomposites obtained by depositing CuO by ADP and WI; the consumption values are compared with the expected ones and the contributions of the single signals are evaluated by fitting procedure.

	H_2 [mol/g] Measured	**H_2 [mol/g] Expected[a]**	**Peak 1 T (°C)**	**Peak 1[b]**	**Peak 2 T (°C)**	**Peak 2[b]**	**Peak 3 T (°C)**	**Peak 3[b]**
$LaCoO_3$	0.0058	0.0061			440	0.0383	600	0.0325
						(66)		(34)
						66		34
Cu10	0.0070	0.0067	323	0.0007	411	0.0038	572	0.0026
				(9)		(54)		(37)
				17		28		55
Cu15	0.0074	0.0070	320	0.0005	420	0.0042	568	0.0027
				(7)		(57)		(36)
				23		26		51
Cu20	0.0074	0.0072	318	0.0022	407	0.0030	563	0.0022
				(30)		(41)		(29)
				29		24		47
Cu30	0.0081	0.0076	387	0.0025	422	0.0038	552	0.0019
				(30)		(47)		(23)
				38		20		41
Cu15 WI	0.0067	0.0070	421	0.0027	430	0.0006	583	0.0014
				(41)		(39)		(20)
				23		26		51

[a] = determined considering the presence of copper as Cu(II) and of cobalt as Co(III).
[b] = first row effective consumption for the specific peak as obtained from fitting procedure; second raw, inside brackets, % of this peak with respect to the total; third raw expected consumption for this peak calculated attributing Peak 1 to Cu(II) →Cu(0), Peak 2 to Co(III) →Co(II) and Peak 3 to Co(II) →Co(0).

Focusing on copper, its reduction seems to follow the expectations for CuO (peak at 310-320°C) but with increasing deposited amount of copper, the reduction temperature increases at 387°C suggesting that, in general, lower reduction temperatures are observed for copper oxide only in case of high dispersion. The increase of the Cu(II) reduction temperature observed in the samples richer in copper confirm this statement.. This is further confirmed by the results obtained on the sample prepared by wet impregnation, in which less dispersed copper oxide is present. In this case the reduction temperatures of cobalt are similar to those observed in $LaCoO_3$ (430°C instead of 440°C for Co(III) to Co(II) and 583°C instead of 600°C for Co(II) to Co(0)) and the Cu(II) reduction is observed at 420°C, so almost simultaneous to Co(III). This behavior can be

explained by the formation of a more compact CuO layer on the perovskite surface resulting in a higher energy requirement for reduction, consistently, in the nanocomposite richer in copper the peak due to the CuO is not observed at 300° C and the signal at about 400°C shows two contributions at 385°C and 420°C suggesting that the reduction of Cu(II) and of Co(III) are almost concomitant. Support effects on the dispersion and reducibility of copper oxide have been documented in the literature [47-48]. A behavior similar to the one observed in this work was also observed by Fang et al. on $CuO/LaCoO_3$ catalysts used for higher alcohol synthesis from syngas [49], whereas a significant decrease of the reduction temperatures of both CuO and of the support was observed in nanocomposites obtained by depositing copper oxide on supports different from $LaCoO_3$ [18, 50-52], suggesting a different interaction mechanism. The different degree of hydroxylation could play a role.

3.4 Catalytic activity

3.4.1 Reactivity with CO + NO

The catalytic tests with CO+NO mixtures were performed using stoichiometric amounts of CO and NO, each at 4 vol % dilution (See Table 2). Figure 3 shows the NO and CO conversions, as well as the yields to N_2 and CO_2 respectively, as a function of temperature for all the catalysts. The yield is defined as:

$$N_2 \text{ yield } (\%) = 0.5 * \text{molar flowrate of } N_2 / \text{molar flowrate of NO fed} * 100 \quad (1)$$

$$CO_2 \text{ yield } (\%) = \text{molar flowrate of } CO_2 / \text{molar flowrate of CO fed} * 100 \quad (2)$$

The higher Cu-loaded samples (Cu15, Cu20 and Cu30) reach total NO conversion at 400°C with a common light-off temperature > 250°C (Figure 3a). The $LaCoO_3$ support, as expected, has no activity in this reaction. Poor activity is also shown by the Cu10 sample, but it is interesting to

notice that, switching from 10% to 15% loaded nanocomposite, there is a remarkable increase in the activity. Further increasing of Cu content does not lead to an enhancement of the activity of the catalyst: on the contrary, Cu10 and Cu20 nanocomposites show higher activity below 300°C with respect to the highest Cu containing sample (Cu30).

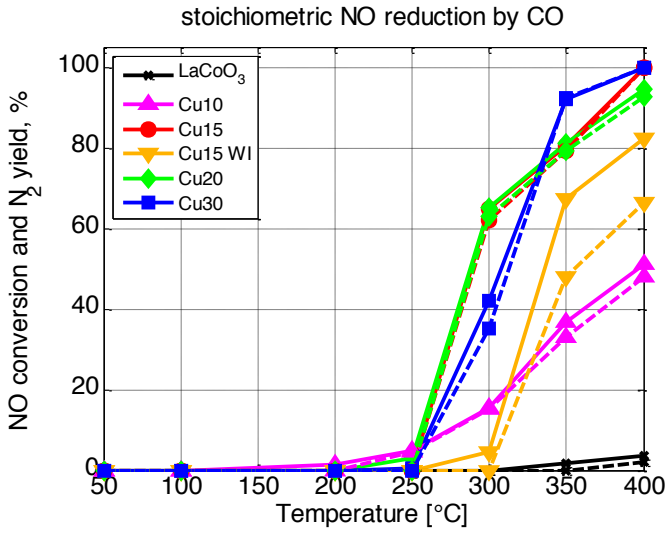

Figure 3:NO conversion and yield to N_2 (a), CO conversion and yield to CO_2 (b) as a function of temperature, obtained for $LaCoO_3$ and $CuO/LaCoO_3$ catalysts in the CO assisted NO reduction; WI indicates the catalyst obtained by wet impregnation, all the other catalysts are prepared by Ammonia Driving Deposition Precipitation. N_2 and CO_2 yields in dashed lines. x $LaCoO_3$; ▲ Cu10; ● Cu15; ▼ Cu15 WI; ♦ Cu20; ■ Cu30

All the ADP samples display an almost perfect match between NO conversion and yield of N_2 (Figure 3a), proving that N_2 is the only reduction product. Similarly, CO conversion matches CO_2 yield (Figure 3b), confirming the direct, quantitative oxidation of CO to CO_2, for any catalyst tested. It must be observed that the sample prepared by wet impregnation (Cu15 WI) shows a N_2 yield lower that NO conversion, Figure 3a. The difference grows with the temperature (thus the extent of reaction). The gap is entirely due to N_2O, whereas NO_2 has not been detected.

These considerations suggest that an optimized composition is needed to obtain the maximum catalytic activity. A synergic effect of copper and perovskite surface may be strictly involved in the reactivity, so an excessive coverage of the support appears not so effective. The comparable activity of Cu15, Cu20 and Cu30 is thus consistent with the diffusion of copper below the surface observed in the characterization studies. The lower activity exhibited by the Cu10 catalyst could be due to the presence of an insufficient amount of copper.

3.4.2 Reactivity with CO + O_2

The catalytic activity in CO oxidation was evaluated using a stoichiometric mixture of CO and O_2 (4 and 2 vol %, respectively). In Figure 4 the CO conversions as a function of temperature achieved by all the nanocomposites prepared and the bare $LaCoO_3$ support are shown. The activity of all the nanocomposite catalysts is very similar to $LaCoO_3$'s one, which is well known to be a good oxidation catalyst [53]. The presence of CuO, deposited on the $LaCoO_3$ surface to enhance the reactivity toward NO reduction, is not detrimental to CO oxidation.

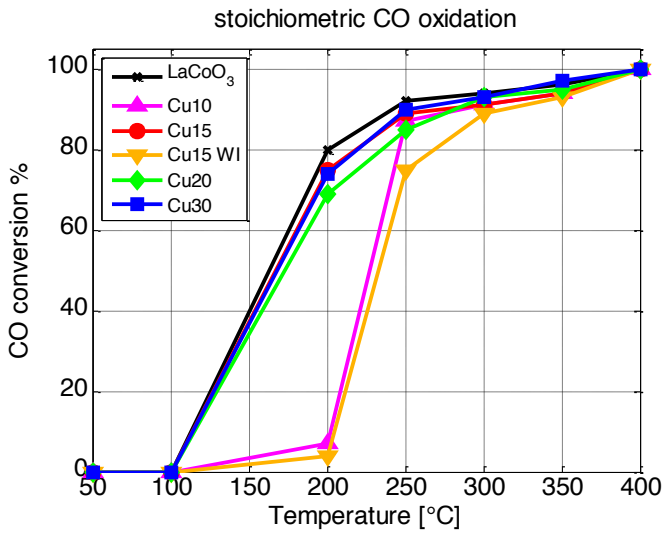

Figure 4: CO conversion as a function of temperature obtained for $LaCoO_3$ and $CuO/LaCoO_3$ catalysts in the CO oxidation; WI indicates the catalyst obtained by wet impregnation, all the other catalysts are prepared by Ammonia Driving Deposition Precipitation.
x $LaCoO_3$; ▲ Cu10; ● Cu15; ▼ Cu15 WI; ♦ Cu20; ■ Cu30

All the materials reach 100% conversion at 400°C and light-off temperature lower than 200°C, except for the Cu10 nanocomposite whose activity is again poorer compared to the other catalysts, apparently because of low active phase content. Again, the catalyst obtained by traditional wet impregnation is less active than the one having the same Cu loading, prepared by ADP.

3.4.3 Reactivity with a synthetic automotive exhaust

The complex mixture (see Table 2) more realistically evaluates the materials' activity, at conditions approaching the effective automotive exhaust. In addition to a larger number of species, including a relevant amount (10 vol %) of steam, we compared the catalysts behavior at both stoichiometric amount of O_2, based on the 'fuels' (i.e. species than can be oxidized), and in a lack of O_2 (fuel rich conditions). With the complex mixture we tested only the catalysts that exhibited substantial differences in activity using the simpler mixtures (Figures 3 and 4), related,

according to the results collected so far, to the existence of an optimum CuO composition. This evidence is better clarified by Figure 5: the conversion of CO in direct oxidation and in CO-assisted NO reduction is plotted against the amount of Cu, at a fixed temperature. To highlight the effect of Cu loading, the reference temperatures were chosen within a range where kinetics is the rate-determing step. Thus, for $CO+O_2$ reaction, the selected temperature is 250°C; 400°C for NO+CO reaction. The catalyst from WI is not considered because of its lower activity in NO reduction (Figure 3a) compared to the ADP-synthetized sample, even at the same Cu loading.

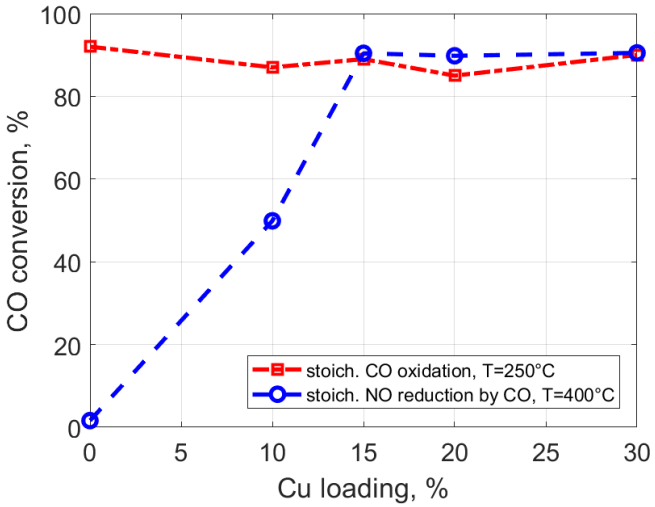

Figure 5: CO conversion as a function of Cu loading, for the stoichiometric $CO+O_2$ oxidation at 250°C (■, red line) and for the stoichiometric CO-assisted NO reduction at 400°C (O, blue line). All samples synthetized by ADP.

As seen in Figure 4, a very high oxidation activity at 250°C is proved by all the samples, despite the presence of Cu, with CO conversion between 85% and 90%, including the case of $LaCoO_3$, i.e. 0% Cu. In addition, the improvement in reducing NO is extremely clear at 400°C (Figure 3). As Cu loading increases from 0% to 15%, a correspondent increase of CO conversion is observed, from 0% to 90%. Higher Cu loadings, i.e. 20 and 30%, to do not appear to affect the

catalytic activity: for this reason, in addition to $LaCoO_3$, Cu10 and Cu15 were the only selected to be tested with complex mixture.

In Figures 6 to 11 we compare the different materials' activity in the removal of each single species within the complex mixture, at both stoichiometric and fuel rich conditions. Note that a different experimental setup and operation mode compared to the simpler mixtures allowed to collect data at a higher frequency, over a larger temperature range (up to 600°C), better spotting the onset of activity.

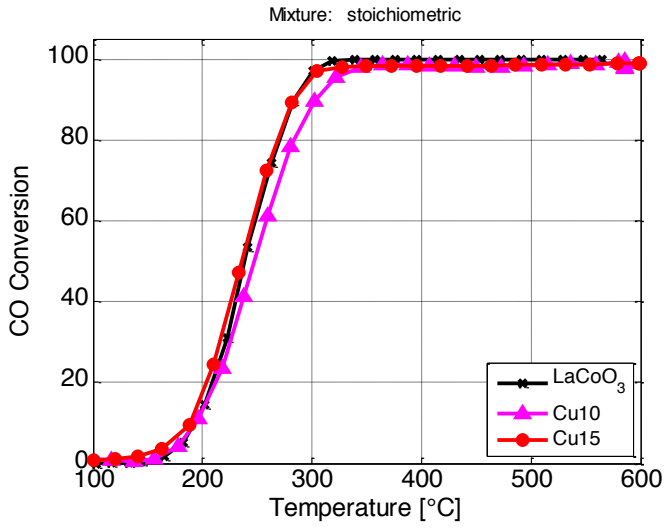

a)

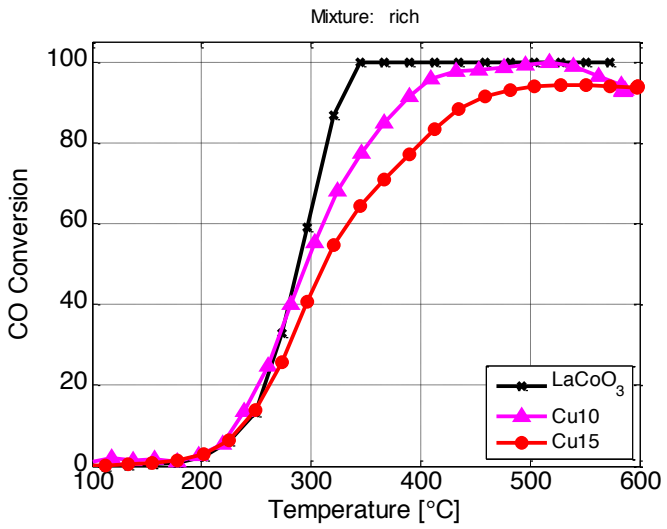

b)

Figure 6. CO conversion as a function of temperature, using synthetic automotive exhaust as feed mixture, at stoichiometric (a) and fuels-rich (b) conditions. x $LaCoO_3$; ▲ Cu10; ● Cu15.

Concerning the CO oxidation shown in Figure 6, the deposition of copper does not affect the activity insofar O_2 is sufficient. Comparing with the simple $CO+O_2$ mixture, Figure 4, the activity in the complex mixture appears to be lower, as reflected by a higher activation temperature (approx. 50°C) notwithstanding the larger contact time (i.e. 1/GHSV) used with the complex mixture. This can be the result of the lower concentrations of CO, which reduces its adsorption rate on active sites. This can be limiting for the overall reaction since CO chemisorption on the perovskite surface is the first step for oxidation. Beyond this, the presence of 10% steam is most likely the responsible for the differences in CO oxidation observed between Figure 4 and Figure 6. In fact, steam was observed to strongly affects the interaction between CO and cobalt oxide surfaces and then the reactivity of Co-containing oxides in CO oxidation [54]. However, note that the activity in CO oxidation at stoichiometric oxygen is the same for all the catalysts, Figure 6a, including Cu10 which was less reactive in the model CO oxidation. This difference could be attributed to the activation treatment carried out by heating in air at 600°C and supports the hypothesis of a lower reactivity of Cu(I) in CO oxidation.

In fuel rich conditions (deficiency of O_2, Figure 6b) we observe a comparable temperature for the onset of activity, irrespective of the Cu loading, but the light off temperature is higher than at stoichiometric conditions, confirming a sort of self-poisoning of the catalyst by the fuels themselves. In this view, the more consistent presence of reductants (HCs, H_2 and CO) under reach conditions could be significant. Moreover, the CO oxidation on metal oxides is supposed to happen through a Mars and van Krevelen mechanism involving the use of perovskite lattice oxygen and this can be more difficult under fuel rich conditions than under stoichiometric ones

[10]. At higher temperature, the conversion of CO increases less, and it is less affected by the temperature increment, as the copper loading increases. In a condition of competition for O_2, CO loses its ease of oxidation in the presence of Cu. That is a clear indication of Figure 6b: at fixed temperatures, in reducing conditions, as Cu loading increases, the CO conversion slightly decreases. Again, the co-reactants and the 'inerts' (steam and CO_2) appear to modify the activity of the catalysts and the role of copper. It is interesting to note that cobalt was observed to facilitate the desorption from a perovskite surface of the CO_2 formed from CO oxidation [55] suggesting that the cobalt presence on the catalyst surface is fundamental for successful oxidation.

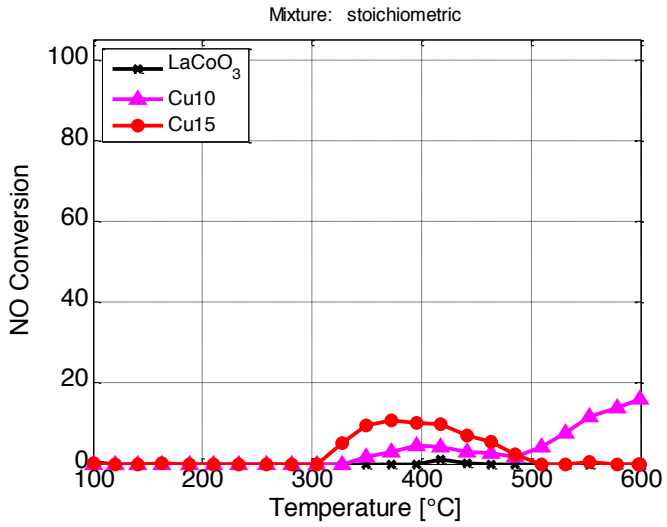

a)

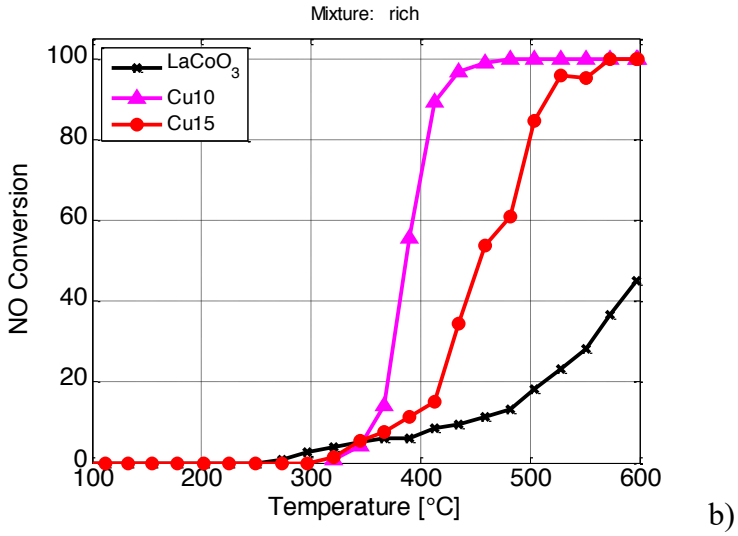

Figure 7. NO conversion as a function of temperature, using synthetic automotive exhaust as feed mixture, at stoichiometric (a) and fuels-rich (b) conditions. x $LaCoO_3$; ▲ Cu10; ● Cu15.

The conversion of NO is presented in Figure 7. It is evident that the presence of O_2 prevents any significant NO reduction. This is consistent with the mechanism proposed for perovskites that considers the interaction between NO and the oxygen vacancies present on the perovskite surface, as the rate determining step for NO reduction [10]. Much better results are achieved under fuel-rich conditions, but the activity is not proportional to the Cu-loading. Cu10 appears more effective in NO reduction than Cu15, allowing 100% NO reduction to be achieved slightly above 400°C. Note that at fuel rich conditions two aspects become relevant: 1) the high dispersion of CuO particles in the Cu10, and 2) the presence of Cu(I), at not-oxidizing conditions [56]. Lu *et al.* [57] already observed, investigating the mechanism of NO reduction on copper in presence of oxygen and isobutene at 770 K, that the CuO needs to be reduced to Cu(I) to activate the NO reduction process. Moreover, they observed that the reductant of NO is not the hydrocarbon, but a reactive intermediate, the aldehydic form, resulting from a partial oxidation of hydrocarbons. This then leads to a reduction of Cu(I) to Cu(0) and a fast consumption of NO. A rapid conversion of NO can only be observed in a narrow range of O_2/HC ratio. A high ratio

leads to deactivation by complete oxidation of the copper surface to Cu(II), inactive in NO reduction. A low ratio limits both the reaction of oxidation of the hydrocarbon and consequently the formation of aldehydic intermediate and finally the conversion of NO. In absence of oxygen, NO is mostly decomposed instead of reacting with the reactive intermediate. The mechanism is even more complex in presence of water [58].

The complex mixture includes H_2, whose consumption is shown in Figure 8. In the presence of O_2, we expect that the H_2 oxidation occurs quite easily, at both feed compositions, and that the increasing amount of Cu makes it even easier (Figure 8a). This is not unexpected, considering the higher activity of copper in H_2 activation with respect to cobalt (confirmed also by the TPR measurements). At fuel rich conditions, the higher reactivity of H_2 consumes the available O_2 at temperature lower than other species. In case of smaller Cu loading (including $LaCoO_3$), the consumption rate is not high enough to deplete the available O_2 before other species (CO, C3s) activate; thus, all O_2 is consumed when H_2 is still available, as evident from Figure 8b. In addition, at higher temperature two other opposite processes are active: the consumption of H_2 used in reducing NO and H_2 production by HCs reforming. The latter process is extremely clear with $LaCoO_3$ at rich conditions (Figure 8b) represented by a drop of H_2 conversion above 450°C. This behavior reflects an emerging contribution of H_2 production in parallel to its consumption processes (oxidation and NO reduction).

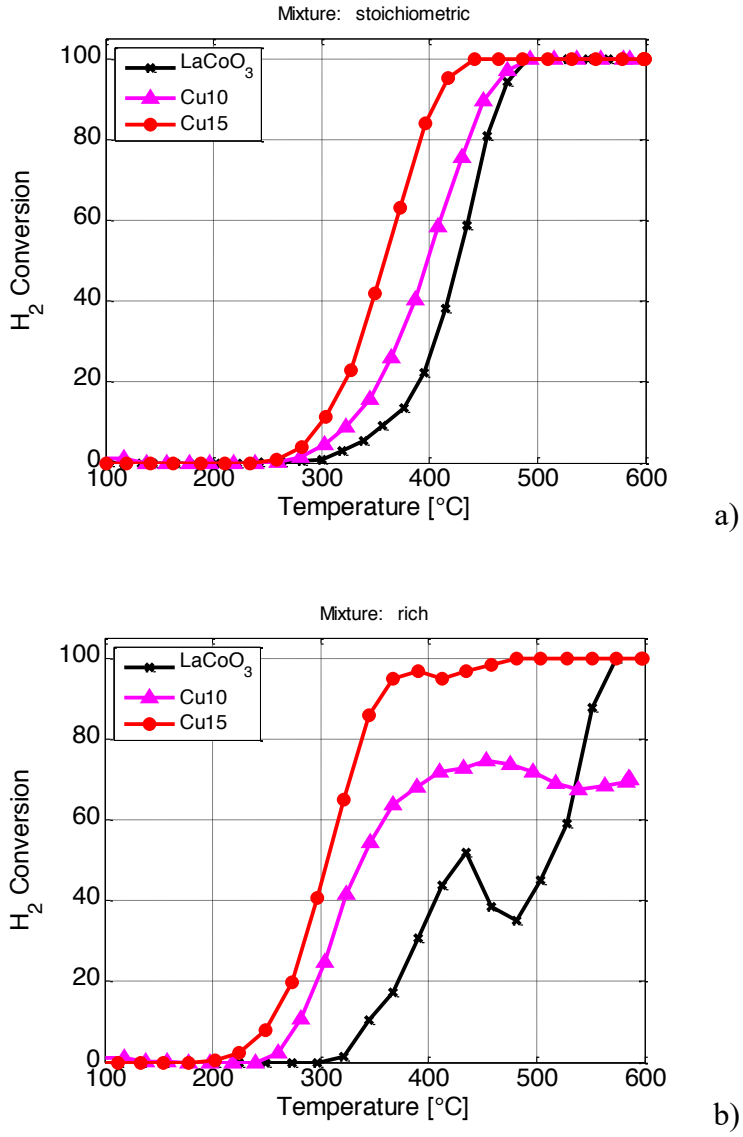

Figure 8. H_2 conversion as a function of temperature, using synthetic automotive exhaust as feed mixture, at stoichiometric (above) and fuels-rich (below) conditions. x $LaCoO_3$; ▲ Cu10; ● Cu15

The onset of reforming is clear also from the C3s conversion profiles (later discussed in Figure 10). Note that CO production by reforming is not reflected in a lowering of CO conversion in Figure 6, because it occurs at such high temperature (when O_2 is totally depleted) that the extra CO produced immediately supports the NO reduction, as proved by the tests on the simple CO+NO mixture (Figure 3).

The HCs (propene, propane and methane) conversion is summarized in Figure 9, at stoichiometric conditions, and Figure 10, for O_2-lean conditions. At stoichiometric conditions, it is clear that unsaturated linear C3 are oxidized more easily (i.e. lower temperature), and the Cu loading slightly improves the ease of activation, proportionally to its amount. At the same time, Cu limits propene total oxidation, even at fairly high temperature: Cu10 has a stronger limitation effect than Cu15. Saturated linear C3 is more difficult to activate, and Cu loading does not help, again limiting the high temperature conversion if present at 10 wt % load. The methane activation remains very limited notwithstanding the high temperature reached and the availability of O_2. In this case, Cu10 suppresses any methane oxidation below 600°C.

Concerning the HCs conversion in O_2-lean mixtures (fuel-rich), Figure 10, the activation of propene dramatically improves with Cu loading, decreasing by some 150°C the onset of measurable conversion compared to $LaCoO_3$. However, the beneficial activity improvement is not duplicate with propane, nor it provides any activity in the CH_4 activation, that remains negligible when O_2 is lacking. When activity is measured, a common pattern emerges, with a maximum of conversion well below 100% at an intermediate temperature, followed by a lowering of conversion. Comparing with the O_2 consumption, shown in Figure 11, we can identify the maximum as the temperature at which O_2 disappears completely. This limits the propene conversion, which must compete for O_2 with the now well-activated CO. C3s conversion increases again at even higher temperature because of the onset of reforming already anticipated.

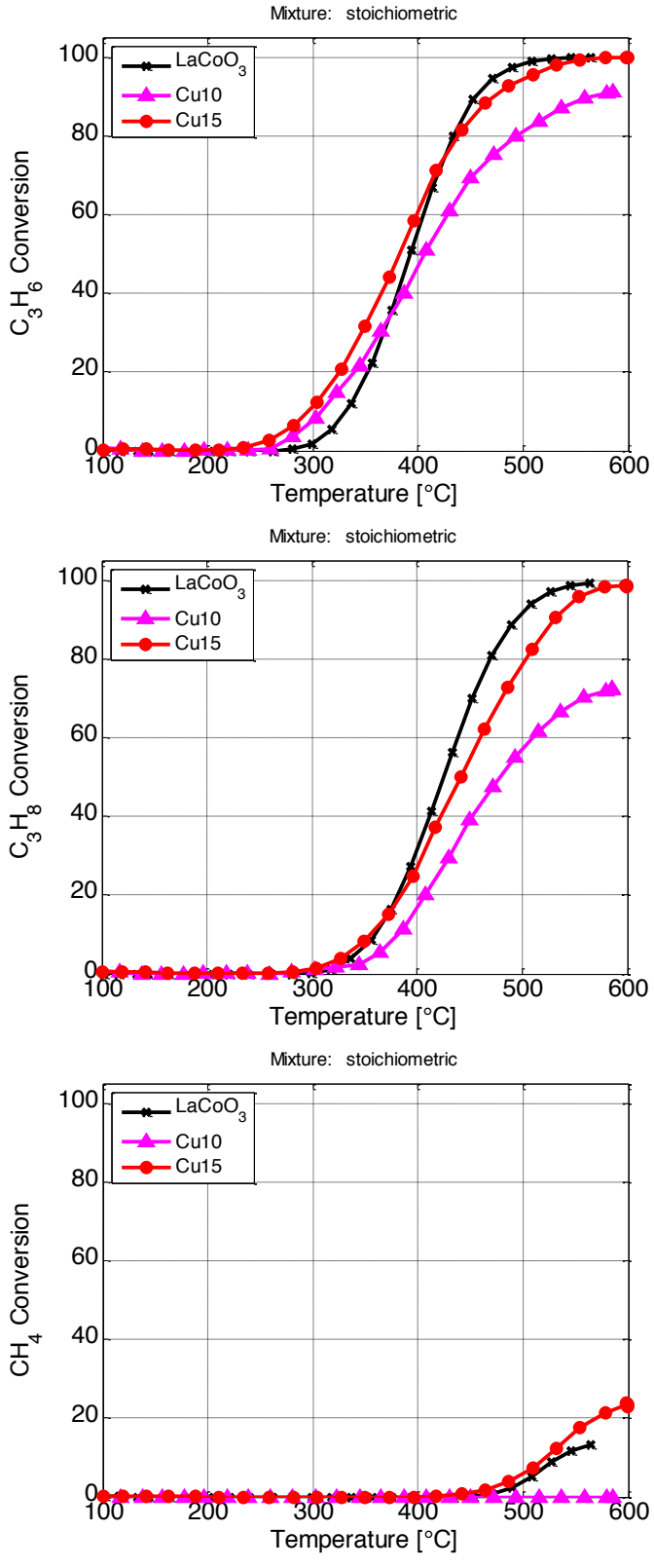

Figure 9. C_3H_6 (a), C_3H_8 (b), and CH_4 (c) conversion as a function of temperature, using synthetic automotive exhaust as feed mixture at stoichiometric conditions. x $LaCoO_3$; ▲ Cu10; ● Cu15.

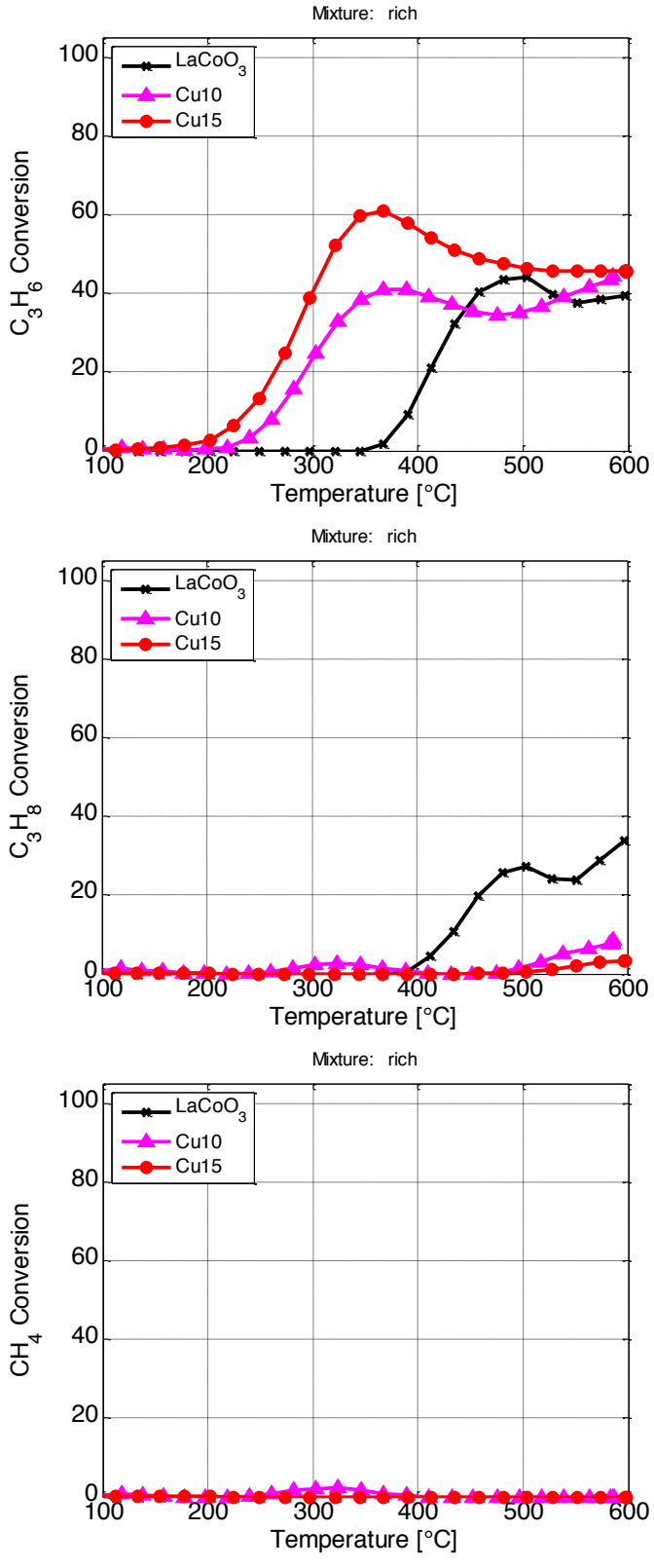

Figure 10. C_3H_6 (a), C_3H_8 (b), and CH_4 (c), conversion as a function of temperature, using synthetic automotive exhaust as feed mixture at fuels-rich conditions. x $LaCoO_3$; ▲ Cu10; ● Cu15.

Finally, Figure 11 shows the O_2 consumption as a function of temperature, which is a key to understand all the results above. We do not observe a remarkable effect of Cu loading at stoichiometric conditions, where Cu loading leads to a very small decrease of O_2 consumption, at any temperature. On the other hand, in O_2-lean mixtures Cu determines a higher consumption of O_2 compared to $LaCoO_3$ between 330°C and 430°C; this is due to $LaCoO_3$ that does not activate the propane oxidation at that temperature, as seen in Figure 10.

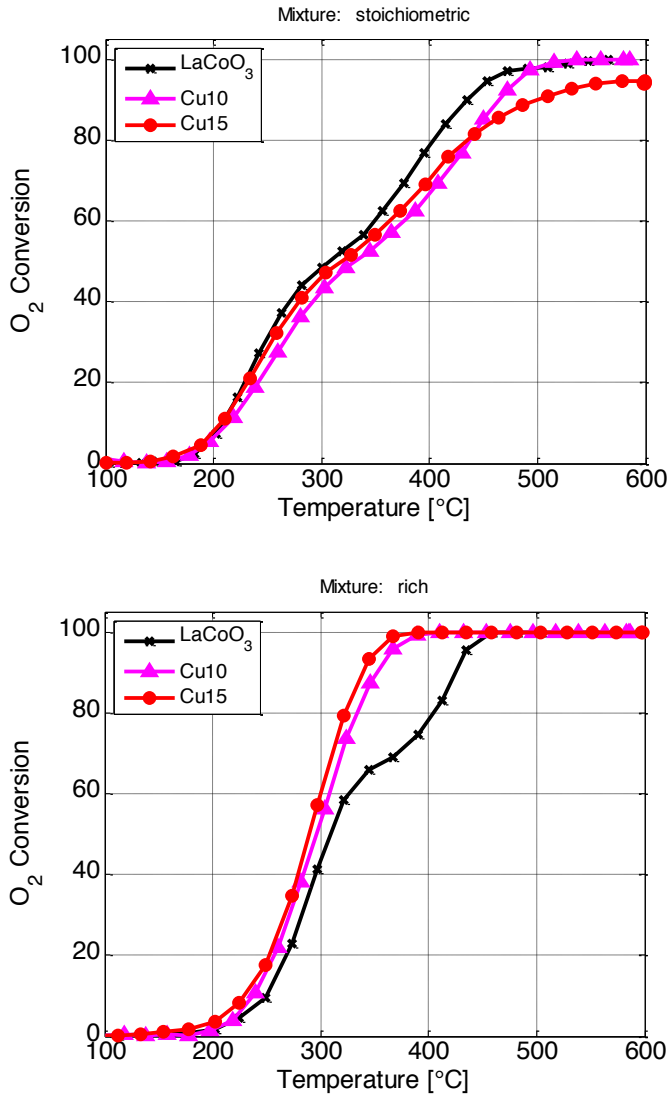

Figure 11. O_2 conversion as a function of temperature, using synthetic automotive exhaust as feed mixture, at stoichiometric (a) and fuels-rich conditions (b). x $LaCoO_3$; ▲ Cu10; ● Cu15.

3.4.4 Comparisons with CuO/$LaNiO_3$

In a previous work [27], we investigated the reactivity of several nanocomposites obtained by depositing an increasing amount of copper oxide on lanthanum nickelate. The preparation of the samples followed the same route used in the present contribution: $LaNiO_3$ was synthetized by means of the citrate method, while the CuO was deposited via ammonia driven deposition precipitation (ADP) method. In both cases the purpose is to combine the bi-functionality given by the reduction properties of copper and the oxidation capability of $LaNiO_3$ and $LaCoO_3$. In Figure 12 we compare the catalytic activity for $LaCoO_3$, Cu10 (LC Cu10), Cu15 (LC Cu15) and for $LaNiO_3$, 15% CuO loaded $LaNiO_3$ (LN Cu15), 30% CuO loaded $LaNiO_3$ (LN Cu30). For this evaluation, the most representative reagents have been chosen: CO and propene for oxidations in stoichiometric conditions and NO reduction for rich ones. The feed mixture is the one approaching actual exhaust composition (Table 2).

CO oxidation is clearly easier on cobaltites than on nickelates (Figure 12a). CuO loading markedly improves the oxidation of nickelates, as already seen [27], bringing the light off temperatures to approx. 180°C like cobaltites (with or without CuO), whereas bare $LaNiO_3$ ignites the combustion of CO at 230°C. Still, $LaNiO_3$-based composites remain less active than those based on $LaCoO_3$, at comparable CuO loading, even less than $LaCoO_3$ itself.

The distinction between the activity of CuO/$LaCoO_3$ and CuO/$LaNiO_3$ observed for CO is confirmed in the oxidation of propene (Figure 12b). The presence of CuO has a positive effect in lowering the ignition temperature only on doped $LaCoO_3$ catalysts. Beside this effect, the activity increase with temperature appears limited by CuO doping on $LaCoO_3$ and less markedly on $LaNiO_3$. As a consequence, the temperature needed to obtain the same conversion among $LaNiO_3$ catalysts increases with CuO loading.

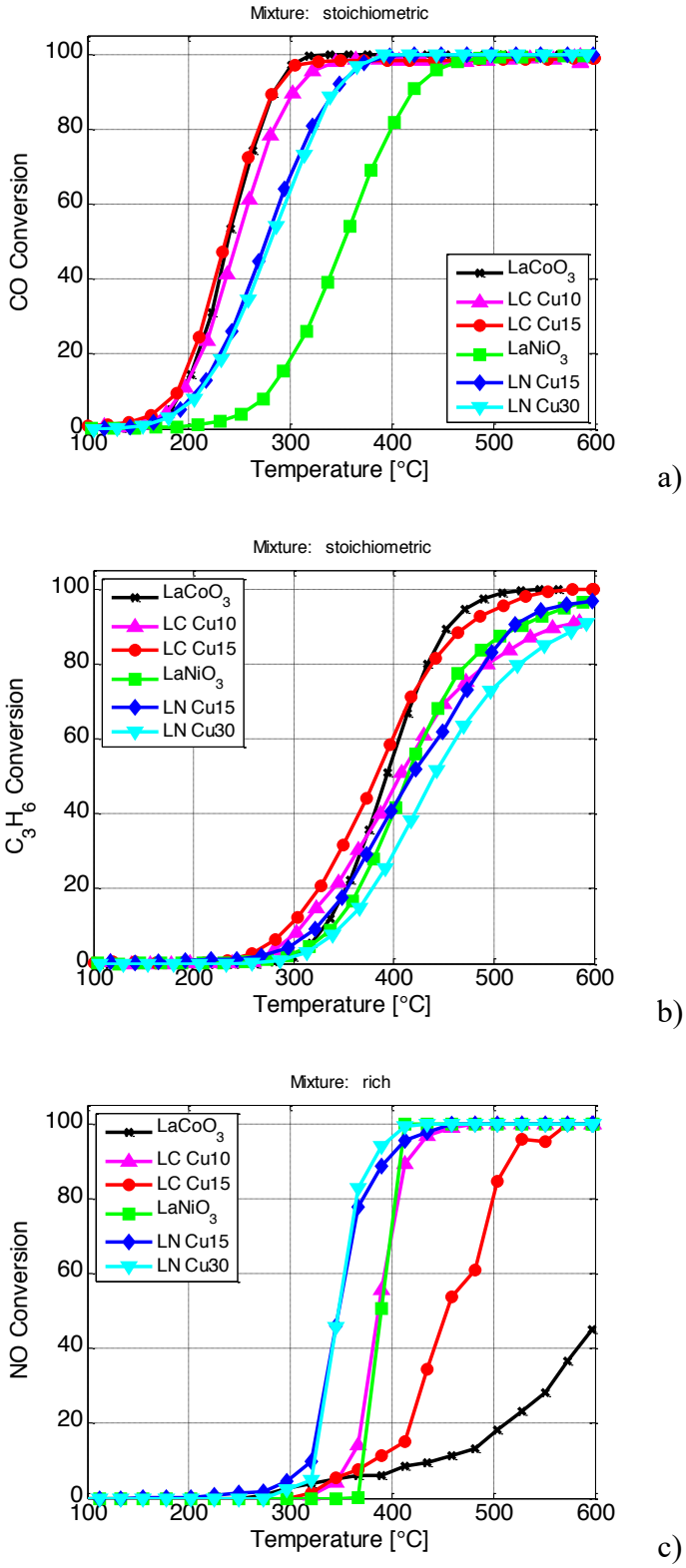

Figure 12. CO conversion (a) and C_3H_6 conversion (b) as a function of temperature at stoichiometric conditions. NO conversion (c) as a function of temperature at fuel-rich conditions. Synthetic automotive exhaust as feed mixture. x $LaCoO_3$; ▲ LC Cu10; ● LC Cu15; ■ $LaNiO_3$; ♦ LN Cu15; ▼ LN Cu30.

We finally compare the NO decomposition obtained while feeding the rich mixture, a requirement to observe the NO reduction, with much less limitations on the reactivity given by the presence of oxygen, as discussed before. From Figure 12c it is evident that $LaCoO_3$ based samples are not able to achieve the consumption of NO until all O_2 is almost completely depleted. At the same time, copper loading greatly enhances the capability of $LaCoO_3$ to reduce NO: temperature needed to obtain 40% NO conversion decreases from 600°C of $LaCoO_3$ to 440°C of LC Cu15 and 380°C of LC Cu10. LC Cu10 is confirmed to be the material that better combines the activity in oxidation with NO reduction capability, as it shows a NO conversion that has a higher dependence from temperature if compared with the other cobaltites, quite similar to $LaNiO_3$. The activity achieved by nickelates however is not replicated by cobaltites: the presence of copper improves further the reactivity in NO reduction on $LaNiO_3$, that is already active itself, lowering the onset of conversion in LN Cu15 and LN Cu30, independently from the amount loaded. We speculate that the different behavior could be associated with the higher activity of the nickelates in steam reforming, producing H_2 that can support NO reduction.

3.4.5 Aging effects

We selected LC Cu10 (i.e. 10% CuO deposited by ADP on $LaCoO_3$) to investigate the effect of aging on this class of nanocomposites. The treatment exposed the catalyst at high temperature twice, each time for 3h, the first at 700°C and the second at 800°C, with intermediate cooling to ambient temperature. The stoichiometric synthetic automotive exhaust mixture (including 10% vol steam) was continuously fed. This is quite challenging for the catalysts. In Table 5 we compared the activity of the fresh and the aged catalyst (LC Cu10) in terms of increment of temperature needed to achieve 10% and 50% of conversion for H_2, CO, O_2, C_3H_6 and C_3H_8, before and after the thermal aging. We observe some activity loss, implying that higher temperature is required to achieve the same performance, after aging. The relative drop of activity is significant for C3s, so that approx. +70°C and +80°C are required to achieve 50% of conversion for C_3H_6 and C_3H_8 respectively. There are evidences that a higher activation energy is needed to catalyze all the oxidations, as confirmed by the positive ΔT associated to O_2; the same activity of the fresh catalyst requires a temperature between 55°C and 64° higher, after the aging treatment. Interestingly, the H_2 oxidation is much less affected by aging, resulting in temperature increments of 34°C and 26°C, to reach 10% and 50% of conversion respectively. The CO consumption, is not uniformly reduced; its light-off is significantly delayed after aging, i.e. +62°C to obtain a conversion of 10%, but the activity after ignition appears much less affected by aging. Indeed, the ΔT_{50} represents the 67% of ΔT_{10}. Finally, the slight activity of LC Cu10 in NO reduction at stoichiometric conditions has been totally lost after thermal aging (data not shown).

Table 5. Measurements of ΔT_{10} and ΔT_{50} for H2, CO, O2, C3H6 and C3H8 between the fresh and the aged Cu10. ΔT = T of aged sample – T of fresh sample.

	ΔT_{10} [°C]	ΔT_{50} [°C]
H_2	34	26
CO	62	43
O_2	55	64
C_3H_6	66	70
C_3H_8	48	80

The activity monitored during the high temperature steps is shown in Figure 13. As expected, the conversion is almost quantitative, particularly at 800°C and stable for most species, with the exception of CH_4 and NO. The conversion of CH_4, always very high at the beginning, drops dramatically. On the other hand, the highest temperature appears to activate some appreciable NO reduction activity.

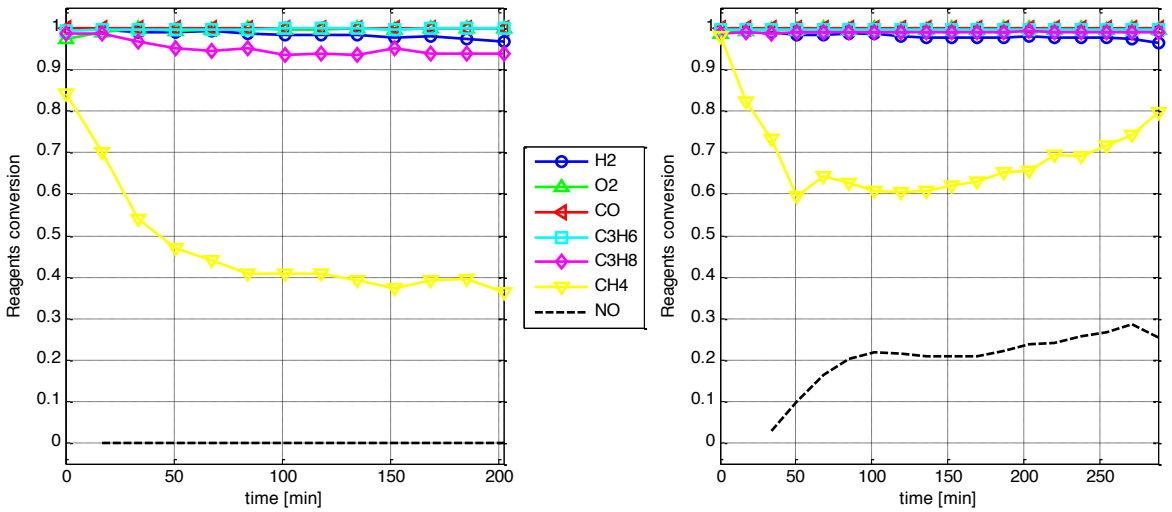

Figure 13. Conversion during aging at 700°C (a) and 800°C (b) on Cu10.

We compared the activity results to the XPS quantitative analysis of the aged material, given the same information on the fresh one. XPS revealed an atomic composition of C on the aged catalytic surface approx. 30% larger than the fresh one, suggesting that coking could be responsible for the loss of activity. The deposition of carbon from the reacting mixture is so slow that it cannot be quantified by the instantaneous C balance, between inlet and outlet, that is always closed within an experimental error of 1.5% for the whole 35-hour treatment. Still, C buildup on the surface proved by XPS can be enough to gradually deactivate the catalytic surface, as reported in Table 5 and support some NO reduction activity.

The XPS analysis on the sample after aging still reveals the presence of Cu(II), but a decrease of copper from 10 % (fresh catalyst – Table 3) to 6% is evident, suggesting a further diffusion of copper in the subsurface layers. This could be very likely responsible for the depletion of the slight activity towards NO obtained by Cu10 in stoichiometric conditions and it is coherent with the reduction capability of $LaCoO_3$.

4. Conclusions

In this paper several composite catalysts prepared by depositing CuO on a $LaCoO_3$ powder have been developed aiming at TWC applications. The nanocomposites have been obtained by means of a new method: the Ammonium-driven Deposition Precipitation (ADP). The procedure allows to obtain a high dispersion of the copper oxide. The samples have been characterized by means of X-Ray Photoelectron Spectroscopy, X-Ray Diffraction, Temperature Programmed Reduction, N_2-Adsorption, Scanning Electron Microscopy, Energy Dispersive X-Ray analysis, Transmission Electron Microscopy, Inductive Coupled Plasma Optical Emission Spectrometry and the obtained results are consistent with a homogeneous deposition of highly dispersed CuO on the

surface of the perovskite. XRD shows that copper oxide is deposited on the perovskite surface and do not enter the crystalline cell. However, when the amount of copper deposited increases beyond a certain limit it tends to diffuse below the surface. The deposition of copper oxide increases the reducibility, as confirmed by TPR, affecting also the reactivity. The reactivity in two model reactions, CO oxidation and CO assisted NO reduction was studied to evaluate the role of the different species. The activity with respect to CO assisted NO reduction increases with Cu loading, without losing activity in CO oxidation: 90-100% NO conversion is observed around 350°C for the nanocomposites richer in Cu. The characterization and reactivity results are compared with those obtained on a composite prepared by means of the traditional wet impregnation procedure, confirming the superior activity of the ADP-prepared catalysts. The activity of some samples ($LaCoO_3$, 10% and 15% Cu loaded $LaCoO_3$) have been also compared using a synthetic, complex mixture reflecting automotive exhaust composition, including 10% steam to evaluate the real applicability of the catalysts in TWC. Interesting differences have been revealed by comparing the activity using simplified and realistic feed mixtures. Cu loading on ADP-prepared samples proved effective in improving propene and H_2 oxidation, particularly in O_2-lean mixture. However, the most important result is a significant improvement of NO reduction activity given by the Cu loading. NO reduction is relevant in O_2-poor mixtures (around 100% at about 400-450°C), even slightly below the stoichiometric. The effects are more pronounced with 10% Cu loading, rather than 15%, suggesting the need to optimize the dispersion procedure. Compared to similar catalysts based on $LaNiO_3$ that we prepared by the same ADP technique [27], we gained in oxidation activity, but the CuO doping is not enough to achieve the same NO reduction activity given by nickelates. The catalysts lose some activity after high temperature aging in steam, most likely because of carbon formation onto the surface

and copper depletion. A combination of Cu-doped $LaCoO_3$ and $LaNiO_3$ may also be an option to take advantage of complementary features.

The obtained results indicate that interesting catalytic performances for TWC applications can be obtained in noble metal free catalysts by means of high dispersion of copper oxide on the surface of perovskites. Although not fully competitive with actual PGM-based TWCs, the materials prepared and tested in this work could be considered downstream of a low-PGM, close-coupled converted, as already successfully proved [59].

ACKNOWLEDGEMENT

This work was supported by the European Union's H2020 under grant agreement no. 686086 PARTIAL PGMs and University of Padova grant N. CPDA124417. We thank Dr. Annalisa Sandon for the ICP measurements and the Laboratory of Microscopy of the Department of Biology, University of Padova for TEM images.

References

[1] M.M. Natile, E. Ugel, C. Maccato, A. Glisenti $LaCoO_3$: effect of synthesis conditions on properties and reactivity Appl. Catal. B: Environ. 72 (2007) 351–362.

[2] W.F. Libby, Promising Catalyst for Auto Exhaust, Science 171 (1971) 499-500.

[3] S.C. Sorenson, J.A. Wronkiewicz, L.B. Sis, G.P. Wirtz, Properties of $LaCoO_3$ as a catalyst in engine exhaust gases, Bull. Am. Ceram. Soc. 53 (1974) 446-449.

[4] L. Lisi, G. Bagnasco, P. Ciambelli, S. De Rossi, P. Porta, G. Russo, M. Turco, Perovskite-Type Oxides: II. Redox Properties of $LaMn_{1-x}Cu_xO_3$ and $LaCo_{1-x}Cu_xO_3$ and Methane Catalytic Combustion J. Solid State Chem. 146 (1999) 176-183.

[5] L. Simonot, F. Garin, G. Maire, A comparative study of $LaCoO_3$, Co_3O_4 and $LaCoO_3$-Co_3O_4: I. Preparation, characterisation and catalytic properties for the oxidation of CO Appl. Catal. B: Environ. 11 (1997) 167-179.

[6] B. Seyfi, M. Baghalha, H. Kazemian, Modified $LaCoO_3$ nano-perovskite catalysts for the environmental application of automotive CO oxidation Chem. Eng. J. 148 (2009) 306-311.

[7] S. Cimino, G. Landi, L. Lisi, G. Russo, Development of a dual functional structured catalyst for partial oxidation of methane to syngas Catal. Today 117 (2006) 454-461.

[8] N. Guilhaume, M. Primet, Three-Way Catalytic Activity and Oxygen Storage Capacity of Perovskite $LaMn_{0.976}Rh_{0.024}O_{3+\delta}$ J. Catal. 165 (1997) 197-204.

[9] P. Doggali, S. Kusaba, Y. Teraoka, P. Chankapure, S. Rayalu, N. Labhsetwar $La_{0.9}Ba_{0.1}CoO_3$ perovskite type catalysts for the control of CO and PM emissions Catal. Comm. 11 (2010) 665-669.

[10] A. Glisenti, M. Pacella, M. Guiotto, M.M. Natile, P. Canu, Largely Cu-doped $LaCo_{1-x}Cu_xO_3$ perovskites for TWC: Toward new PGM-free catalysts Appl. Catal. B: Environ. 180 (2016) 94-105.

[11] N. Tien-Thao, H. Alamdari, M.H. Zahedi-Niaki, S. Kaliaguine $LaCo_{1-x}Cu_xO_{3-\delta}$ perovskite catalysts for higher alcohol synthesis Appl. Catal. A: Gen. 311 (2006) 204-212.

[12] R. Zhang, A. Villanueva, H. Alamdari, S. Kaliaguine, Reduction of NO by CO over nanoscale $LaCo_{1-x}Cu_xO_3$ and $LaMn_{1-x}Cu_xO_3$ perovskites J. Mol. Catal. *A* 258 (2006) 22-34.

[13] C. Zhou, X. Liu, C. Wu, Y. Wen, Xue, Y.R. Chen, Z. Zhang, B. Shan, H. Yin, W.G. Wang, NO oxidation catalysis on copper doped hexagonal phase $LaCoO_3$: a combined experimental and theoretical study Phys. Chem. Chem. Phys. 16 (2014) 5106-5112.

[14] N. Tien Thao, H. Alamdari, S. Kaliaguine, Characterization and reactivity of nanoscale $La(Co,Cu)O_3$ perovskite catalyst precursors for CO hydrogenation J. Sol. State. Chem. 181 (2008) 2006-2019.

[15] M. Navarro, M.A. Peña, J.L.G. Fierro, Hydrogen Production Reactions from Carbon Feedstocks: Fossil Fuels and Biomass Chem. Rev. 107 (2007) 3952-3991.

[16] C.-Y. Lu, W.-C. Chang, M.-Y. Wey, CuO/CeO_2 catalysts prepared with different cerium supports for CO oxidation at low temperature Mater. Chem. Phys. 141 (2013) 512-518.

[17] S. Zeng, Y. Wang, S. Ding, J.J.H.B. Sattler, E. Borodina, L. Zhang, B.M. Weckhuysen, H. Su, Active sites over CuO/CeO_2 and inverse CeO_2/CuO catalysts for preferential CO oxidation J. Power Sources 256 (2014) 301-311.

[18] C. Tang, J. Sun, X. Yao, L. Liu, C. Ge, F. Gao, L. Dong Efficient fabrication of active $CuO\text{-}CeO_2$/SBA-15 catalysts for preferential oxidation of CO by solid state impregnation Appl. Catal. B: Environ. 146 (2014) 201-212.

[19] A.K. Ahmed, A.A. Zuhairi, M.A. Rahman, Recent development in catalytic technologies for methanol synthesis from renewable sources: A critical review Renewable and Sust. Energy Rev. 44 (2015) 508-518.

[20] S.G. Jadhav, P.D. Vaidya, B.M. Bhanage, J.B. Joshi, Catalytic carbon dioxide hydrogenation to methanol: A review of recent studies Chem. Eng. Research and Design 92 (2014) 2557–2567.

[21] X. Guo, A. Yin, W.L. Dai, One pot synthesis of ultra-high copper contented Cu/SBA-15 material as excellent catalyst in the hydrogenation of dimethyl oxalate to ethylene glycol Catal. Lett. 132 (2009) 22-27.

[22] L. C. Daemme, R. de Arruda Penteado, K. C. C. Silva, M. R. Errera, F. M. Z. Zotin, Regulated and Non-Regulated Emissions from a Light-Duty Diesel Car Fueled with Different Diesel Sulfur Content, SAE Technical Paper 2014-36-0110 (2014) 1-10.

[23] N. Thompson, R. Stradling, P. J. Zemroch, P., R. de Craecker, T. Sams, A. Neunteufel, Fuel Effects on Regulated Emissions From Advanced Diesel Engines and Vehicles, SAE Technical Paper 2004-01-1880 (2004) 1-13.

[24] H. Nishioka, K. Yoshida, T. Asanuma, T. Fukuma, Development of Clean Diesel NOx After-treatment System with Sulfur Trap Catalyst, SAE Int. J. Fuels Lubr. 3 (2010) 30-36.

[25] J.R. Gonzalez-Velasco, J.A. Botas, R. Ferret, M.P. Gonzalez-Marcos, J.L. Marc, M.A. Gutierrez-Ortiz, Thermal aging of Pd/Pt/Rh automotive catalysts under a cycled oxidizing-reducing environment, Catalysis Today, 59 (2000) 395-402.

[26] K. Ramanathan, S.H. Oh Chem. Eng. Research and Design. 92 (2014) 350-361.

[27] G. Perin, J. Fabro, M. Guiotto, Q. Xin, M.M. Natile, P. Cool, P. Canu, A. Glisenti, Cu@LaNiO3 based nanocomposites in TWC applications, App. Cat. B: Env., 209 (2017) 214-227.

[28] D.A. Shirley, High-resolution X-ray photoemission spectrum of the valence bands of gold Phys. Rev. B 5 (1972) 4709-4714.

[29] J.F. Moulder, W.F. Stickle, P.E. Sobol, K.D. Bomben, Handbook of X-ray Photoelectron Spectroscopy*;* Chastain, J. Ed., Physical Electronics, Eden Prairie, MN, 1992.

[30] D. Briggs, J.C. Riviere, in: D. Briggs, M.P. Seah (Eds.), Practical Surface Analysis, Wiley, New York, 1983.

[31] M.M. Natile, F. Poletto, A. Galenda, A. Glisenti, T. Montini, L. De Rogatis, P. Fornasiero, $La_{0.6}Sr_{0.4}Co_{1-y}Fe_yO_{3-\delta}$ Perovskites: Influence of the Co/Fe Atomic Ratio on Properties and Catalytic Activity toward Alcohol Steam-Reforming Chem. Mater. 20 (2008) 2314-2327.

[32] A. Galenda, M.M. Natile, V. Krishnan, H. Bertagnolli, A. Glisenti, LaSrCoFeO and Fe_2O_3/LaSrCoFeO powders: Synthesis and characterization *Chem. Mater.* 19 (2007) 2796-2808.

[33] A. Galenda, M.M. Natile, L. Nodari, A. Glisenti, $La_{0.8}Sr_{0.2}Ga_{0.8}Fe_{0.2}O_{3-\delta}$: Influence of the preparation procedure on reactivity toward methanol and ethanol Appl. Catal. B: Environ. 97 (2010) 307-322.

[34] M. Machova, N. Braskova, P. Ivanov, J.B. Carda, V. Kozhukharov, Surface behavior of Sr-doped lanthanide perovskites Appl. Surf. Sci. 119 (1997) 127-136.

[35] P.A.W. van der Heide, Systematic x-ray photoelectron spectroscopic study of La1− xSrx-based perovskite-type oxides Surf. Interface Anal. 33 (2002) 414-425.

[36] NIST XPS Database 20, Version 3.4 [Web Version].

[37] Y. Uwamino, T. Ishizuka, H. Yamatera, X-ray photoelectron spectroscopy of rare-earth compounds J. Electron Spectrosc. Relat. Phenom. 34 (1984) 67-78

[38] T.L. Barr, An ESCA study of the termination of the passivation of elemental metals J. Phys. Chem. 82 (1978) 1801-1810.

[39] M.A. Peña, J.L.G. Fierro Chemical structures and performance of perovskite oxides Chem. Rev. 101 (2001) 1981-2018 and references therein.

[40] R. Lago, G. Bini, M.A. Pena, J.L.G. Fierro, Partial oxidation of methane to synthesis gas using $LnCoO_3$ perovskites as catalyst precursors J. Catal. 167 (1997) 198-209.

[41] J.L.G. Fierro, Structure and composition of perovskite surface in relation to adsorption and catalytic properties Catal. Today 8 (1990) 153-174.

[42] L. Bedel, A.C. Roger, C. Estournes, A. Kiennemann, CoO from partial reduction of La (Co, Fe)O_3 perovskites for Fischer–Tropsch synthesis Catal. Today 85 (2003) 207-218.

[43] L.B. Sis, G.P. Wirtz, S.C. Sorenson, Structure and properties of reduced $LaCoO_3$ J. Appl. Phys. 44 (1973) 5553-5559.

[44] B. Echchahed, S. Kaliaguine, H.S. Alamdari, Well Dispersed CoO by Reduction of $LaCoO_3$ Perovskite Int. J. Chem. React. Eng. 4 (2006) Art. Number A29.

[45] J.L.G. Fierro, M. LoJacono, M. Inversi, P. Porta, R. Lavecchia, F. Cioci, A study of anomalous temperature-programmed reduction profiles of Cu_2O, CuO, and CuO-ZnO catalysts J.Catal. 148 (1994) 709-721.

[46] A. Glisenti, A. Galenda, M.M. Natile Steam reforming and oxidative steam reforming of methanol and ethanol: The behaviour of $LaCo_{0.7}Cu_{0.3}O_3$ Appl. Catal. A 453 (2013) 102-112.

[47] W.-P. Dow, T.-J. Huang, Effects of oxygen vacancy of yttria-stabilized zirconia support on carbon monoxide oxidation over copper catalyst J. Catal. 147 (1994) 322-332.

[48] W.-P. Dow, Y.-P. Wang, T.-J. Huang, Yttria-stabilized zirconia supported copper oxide catalyst: I. Effect of oxygen vacancy of support on copper oxide reduction J. Catal. 160 (1996) 155-170.

[49] Y. Feng, Y. Liu, W. Deng, J. Liu, Cu-Co bi-metal catalyst prepared by perovskite $CuO/LaCoO_3$ used for higher alcohol synthesis from syngasOriginal J. Energy Chemistry 23 (2014) 527-534.

[50] Z. Wu, H. Zhu, Z. Qin, G. Wang, L. Huang, J. Wang, Preferential oxidation of CO in H_2-rich stream over $CuO/Ce_{1-x}Ti_xO_2$ catalysts Appl. Catal. B Env. 98 (2010) 204-212.

[51] J.-L. Cao, Y. Wang, G. Sun, Z.-Y. Zhang, $CuO/Ce_xSn_{1-x}O_2$ catalysts: synthesis, characterization, and catalytic performance for low-temperature CO oxidation Transition Met. Chem. 36 (2011) 107-112.

[52] L. Dong, Y. Tang, B. Li, L. Zhou, F. Gong, H. He, B. Sun, C. Tang, F. Gao, L. Dong, Influence of molar ratio and calcination temperature on the properties of $Ti_xSn_{1-x}O_2$ supporting copper oxide for CO oxidation Appl. Catal. B. Env. 180 (2016) 451-462.

[53] H. Taguchi, S. Yamada, M. Nagao, Y. Ichikawa, K. Tabata, Surface characterization of $LaCoO_3$ synthesized using citric acid Mat. Res. Bull. 37 (2002) 69-76.

[54] F. Grillo, M.M. Natile, A. Glisenti, Low temperature oxidation of carbon monoxide: the influence of water and oxygen on the reactivity of a Co_3O_4 powder surface Appl. Catal. B: Env. 48 (2004) 267-274.

[55] S. Carlotto, M.M. Natile, A. Glisenti, A. Vittadini, Adsorption of CO and formation of carbonates at steps of pure and Co-doped $SrTiO_3$ surfaces by DFT calculations Appl. Surf. Sci. 364 (2016) 522-527.

[56] G. Centi, S. Perathoner, Nature of active species in copper-based catalysts and their chemistry of transformation of nitrogen oxides Appl. Catal. A: Gen. 132 (1995) 179-259.

[57] H. Lu, C.-M. Pradier, A.S. Flodström, Catalytic reduction of nitric oxide on copper. Part I J. Mol. Catal. A. Chem. 112 (1996) 447-457.

[58] H. Lu, C.-M. Pradier, U.O. Karlsson, Catalytic reduction of nitric oxide over copper: Part III: Influence of water vapour J. Mol. Catal. A. Chem. 138 (1999) 227-236.

[59] H. Nakayama, Y. Kanno, M. Nagata, X. Zheng, Development of TWC and PGM Free Catalyst Combination as Gasoline Exhaust Aftertreatment, SAE Int. J. Engines 9 (2016) 2194-2200.